Pergamon

Cement and Concrete Research 32 (2002) 1301–1311

CEMENT AND CONCRETE RESEARCH

Porosity of recycled concrete with substitution of recycled concrete aggregate An experimental study

José M.V. Gómez-Soberón*

3 Sur #503 Cd. Serdán, Puebla, CP 75520, Mexico

Received 8 June 2001; accepted 5 March 2002

Abstract

In this paper, we present the experimental analysis of samples of recycled concrete (RC) with replacement of natural aggregate (NA) by recycled aggregate originating from concrete (RCA). The results of the tests of mechanical properties of RC were used for comparison with tests of mercury intrusion porosimetry (MIP), in which the distribution of the theoretical pore radius, critical pore ratio, the surface area of the concrete, threshold ratio and average pore radius were studied at ages of 7, 28 and 90 days. The results showed some variation in the properties of the RC with respect to ordinary concrete. Porosity increases considerably when NA is replaced by RCA. Additionally, a reduction in the mechanical properties of the RC is seen compared with ordinary concrete when porosity increases.

Keywords: Compressive strength; Porosity; Recycled concrete; Recycled concrete aggregate; Young's modulus

1. Introduction

Current studies of recycled concrete (RC), with partial substitution of natural aggregate (NA) by recycled aggregate originating from concrete (RAC), promise a feasible path for its application, thus satisfying a need, saving energy, improving environmental conditions and providing a solution for the 200 million tons/year of construction waste generated in the EU [1–7].

RCs can be regarded as porous concretes, having permeability values that are twice those of ordinary concretes. Their general behavior shows a decrease in their mechanical and physical properties as the percentage of replacement of NAs by RCA increases [8]. It is also widely accepted that there is an inverse correlation between the volume of pores and the levels of stress to which the concrete can be subjected, and this relationship should also take into account the distribution of the sizes of the pores and the interconnection between them [9–11].

Tests of mercury intrusion porosimetry (MIP) in RC show increases in the total volume of pores, especially in larger pores (> 100 nm). This suggests that this property is a function of both the age of the concrete and the amount of mortar that the RCA contains [12].

Five types of concrete are presented in this work with different RCA contents, together with the behavior of the concrete that provided the RCA, and were prepared for the study of the properties of both the aggregates and the concretes.

2. Experimental

2.1. Original concrete

In this study, 4 m^3 of original concrete (OC) was used. The concrete was made in a mixer and was poured into wooden formwork frames measuring 0.40×0.20×0.10 m. Fifty cylinders measuring ∅ 0.15×0.30 m, eight measuring ∅ 0.15×0.45 m and four cubes measuring 0.10×0.10 m were also used to study the porosity, mechanical behavior, shrinkage and creep.

* L'Hospitalet de Llobregat, Av. Carrılet #338 5-3, Barcelona 08901 Spain. Tel.: +34-933-37-05-69; fax: +34-934-01-72-62.

E-mail address: jmv115@hotmail.com (J.M.V. Gómez-Soberón).

0008-8846/02/$ – see front matter
PII: S0008-8846(02)00795-0

Table 1
Mixtures used for OC

Component	OC
Cement (kg/m^3)[a]	380
Water (kg/m^3)	168
Fine gravel (5–12) (kg/cm^3)[b]	252
Gravel (12–20) (kg/cm^3)[b]	773
Sand (0–5) (kg/m^3)[b]	784
W/C	0.44
Coarse A/Fine A (vol)	1.3
Additives (plastifier)	2.69

[a] CEM I 42.5 R.
[b] Limestone aggregate, Garraf quarry, Barcelona.

Twenty-four hours after pouring, the samples were removed from the formwork and submitted to a curing process for 150 days (see Table 1, in which the specific characteristics of this concrete are given). The specimens were then passed once through a semifixed roller grinder with an inlet width of 0.45 m and a maximum outlet size of 0.025 m. Finally, the resulting material was classified into sizes (mm in all cases): 0–5, 5–10, 10–20, 20–25. The 5–10 and 10–20 fractions were used as RCA in this work.

2.2. Recycled aggregate and NA

The designation used by sizes was: for RCA, gravel 10–20 and fine gravel 5–10; and for the NA, gravel 12–20 and fine gravel 5–12.

The criterion used for this fit was the compacted maximum density (which reduced the possible influences of different particle size). These were:

- For RCA, the combination was 55% gravel and 45% fine gravel.
- For NA, the combination was 70% gravel and 30% fine gravel.

Table 2 shows the properties of the aggregate used. The total porosity to water is the variable that shows the greatest difference between the RCA and NA and, in the worst case, reaches 2.82% for the NA and 14.86% for the fine gravel fraction of the RCA. As regards density, the RCA is lighter than the NA (with an average of 14% less in D_s and 9% less in D_{sss}) The RCA shows an increase in density, which is directly proportional to the greater particle size. Finally, the differences between dry and dry surface saturated conditions are greater for the RCA than for the NA.

The RCA used in this study can be considered as being within the RILEM recommendation for Type II RCA (absorption $\leq$10% and $D_s \geq 2000$ kg/m^3). For the Belgian recommendation, they are GBSBII (absorption <9% and D_s>2100 kg/m^3) and in the Japanese case they comply with the absorption requirement ($\leq$7% and $D_s \geq 2200$ kg/m^3) in the fractions used [13–16]. Consequently, the RCA employed in this study may be used in both plain and reinforced concrete if its application and factors of behavior are taken into account.

2.3. Mix of RCs

Due to the difficulty in determining the real water/cement (W/C) ration because of the high variation of absorption in the RCA, it was decided to use basic ACI 211.1 and ACI 211.2 mix concepts in accordance with the following criteria.

(1) The substitution of NA by RCA was done using equal volume fractions with the following condition:

$$r = \mathrm{RCA}_{\mathrm{coarse}}/(\mathrm{RCA}_{\mathrm{coarse}} + \mathrm{NA}_{\mathrm{coarse}})$$

$$(0.00 \leq r \leq 1.00)$$

where: r=percentage of NA replaced by RCA, by volume; $\mathrm{RCA}_{\mathrm{coarse}}$=55% recycled gravel+45% recycled fine gravel; and $\mathrm{NA}_{\mathrm{coarse}}$=70% natural gravel+30% natural fine gravel.

The percentages of the five studied samples of RC were: r=0.00, 0.15, 0.30, 0.60 and 1.00. As fine aggregate, 100% crushed natural limestone sand from the Garraf quarry (Barcelona) was used.

(2) The RCA showed an increase in absorption proportional to the time spent in water. The time allowed for the mixture was 20 min of immersion, with up to 97% fine gravel and 77% gravel, in all cases with comparison after 24 h.

Table 2
Properties of recycled aggregate and NA

	RCA			NA[a]		
Property	10–20	5–10	0–5	12–20	5–12	0–5
Dry specific gravity (kg/m^3)	2280	2260	2170	2570	2640	2570
Specific gravity (surface dry) (kg/m^3)	2410	2420	2350	2590	2670	2600
Water absorption (%)	5.828	6.806	8.160	0.876	1.134	1.49
Total porosity (%)	13.42	14.86	–	2.70	2.82	–
Shape coefficient	0.363	0.466	–	0.364	0.576	–
Longs indices	6	15	–	8	19	–
Modulus of fineness	7.2	6.2	3.8	6.9	5.0	3.3
Sand equivalent (%)	–	–	93.6	–	–	93.8
Particles <200 μm (%)	0.06	0.29	9.85	0.50	2.46	9.24

[a] Limestone aggregate, Garraf quarry, Barcelona.

Table 3
Mixtures used for RC

Component		r=1.00	r=0.60	r=0.30	r=0.15	r=0.00
Cement (kg/m^3)[a]		400				
Water (kg/m^3)		207.6				
RCA (kg/cm^3)	Fine gravel (5–10)	406	258	134	69	0
	Gravel (10–20)	497	315	164	84	0
NA (kg/cm^3)	Fine gravel (5–12)[b]	0	268	488	604	710
	Gravel (12–20)[b]	0	115	209	259	304
Sand (0–5) (kg/m^3)[b]		662				
W/C		0.52				
Coarse A/Fine A (vol)		1.53				

[a] CEM I 52.5R UNE 80 301 96 RC/97.
[b] Limestone aggregate, Garraf quarry, Barcelona.

(3) The amount of water absorbed by the aggregate was taken into account separately, in addition to its wetness before mixing and the free water that formed part of the mixture. The above aspect is justified by criteria that were emphasized in a previous publication of the authors [17–20].

With the established mixing time and the required amount of water, the order of mixing the materials guaranteed (as far as possible) the immobility of the water and an improvement in the transition zone. The following sequence was adopted: (a) all of the coarse aggregates and water were introduced into the mixer; (b) these were mixed for 2 min; (c) the mixer was switched off for 3 min; (d) stages (b) and (c) were repeated twice; (e) the cement was introduced and mixed for 3 min; and (f) the sand was added and mixed for another 3 min.

The mixes obtained using the above criteria are given in Table 3. As can be seen, the variation in consistency and volumetric weight for the different percentages of aggregate replaced is within tolerable limits (slump 0.1±0.03 m and concrete with volumetric weight normal).

2.4. Properties of the concretes

The tests on the different concretes comprised the study of the physical properties such as absorption, density, porosity and water permeability; and mechanical properties such as compression, tensile strength, Young's modulus, shrinkage and creep.

Tests of the physical properties of the concrete were carried out on 0.10×0.10 m cubic samples, while the mechanical tests were done on ∅ 0.15×0.30 m (compression, tensile strength and Young's modulus) and ∅ 0.15×0.45 m cylindrical (shrinkage and creep) samples with ages of 7, 28 and 90 days, and 179, 200 and 262 for RC. Tables 4 and 5 show the results of the tests, in which the Spanish UNE [21–33] and ASTM standards were used. Each value in the table is the average of two tests for physical properties and an average of three for the mechanical tests (two for shrinkage and creep).

The sections below provide a summary of the behavior of the physical and mechanical properties.

2.4.1. Physical properties

The absorption of the RC increases proportionally with RCA content, while the density decreases slightly. Water porosity, like absorption, increases proportionally with RCA content. The above comments are presented in Table 4.

2.4.2. Mechanical properties

Simple compression decreases as the r factor increases for the studied ages: when $r \leq 0.30$, f_c' is appreciably the same as the reference concrete, and if the evolution of f_c' is compared with the age of the RC, it is seen that its behavior is the same as the reference concrete, although the stress levels are of course lower. Indirect stress shows a similar evolution with age as with ordinary concretes. However, samples with r=0.60 and r=1.00 show tensile strength values that are appreciably lower than the rest of the studied concretes for the age range under study. Finally, comparing results without reference to the age of the test, Young's modulus shows its minimum value for r=0.60, closely followed by the value for r=1.00. This property,

Table 4
Mechanical and physical properties of RC

Age[a]	Tensile strength (MPa)			Compressive strength (MPa)			Young's modulus (GPa)			Absorption	Water porosity	D_s	D_{sss}
factor	7	28	90	7	28	90	7	28	90	(%)	(%)	(kg/m^3)	(kg/m^3)
r=0.00	3.6	3.7	3.9	33.3	39.0	42.1	27.6	29.7	32.4	8.40	18.0	2130	2310
r=0.15	3.3	3.7	3.9	33.9	38.1	41.6	27.2	291	30.1	8.60	18.5	2140	2360
r=0.30	3.3	3.6	3.9	34.8	37.0	39.5	26.5	27.8	29.4	8.60	18.5	2150	2330
r=0.60	3.2	3.4	3.7	30.6	35.8	38.3	25.5	26.6	27.6	9.00	19.2	2120	2320
r=1.00	3.5	3.3	3.6	30.7	34.5	37.5	26.9	26.7	26.4	9.60	20.1	2090	2290
OC	3.2	3.8	–	35.2	38.4	–	33.0	33.7	–	5.90	13.4	2270	2410
OC[b]	4.1	4.1	4.2	45.1	45.4	47.0	35.2	34.5	34.6				

[a] Days.
[b] At 172, 179, and 262 days of age.

Table 5
Shrinkage and creep of RC

Component properties		r=1.00	r=0.60	r=0.30	r=0.15	r=0.00	OC
f_c' (28 days) (MPa)		34.5	35.8	37.0	38.1	38.8	38.4[a]
Stress level for creep (MPa)[b]		12.08	12.53	12.95	13.34	13.58	13.44
$\varepsilon_{sh\ basic}$ (mm/m)		0.0138	0.0310	−0.0040	−0.0800	−0.0220	−0.0260[c]
$\varepsilon_{sh\ drying}$ (mm/m)		0.4029	0.4104	0.3524	0.3763	0.3740	0.1940[c]
$\varepsilon_{c\ basic}$	Instantaneous (mm/m)	0.1370	0.1470	0.1645	0.1350	0.1430	0.1180[c]
	φ (90_{days}, t_0)	0.85	0.72	0.55	0.81	0.44	0.34[c]
$\varepsilon_{c\ drying}$	Instantaneous (mm/m)	0.1580	0.1530	0.1380	0.1350	0.1600	0.1265[c]
	φ (90_{days}, t_0)	4.04	3.85	3.65	3.55	2.90	1.67[c]

[a] The age of the test was 200 days.
[b] $0.35f_c'$.
[c] Shrinkage (262 and 172 days) and φ (262 and 172 days).

therefore, shows a similar behavior to ordinary concretes (see Table 4).

For the shrinkage and creep tests, the samples, after 28 days in a curing chamber (T=20±2 °C and RH=90±5%), were submitted to a climatic chamber (T=20 °C and RH=50%) for 90 days. The specimens used for basic shrinkage and creep measurement were sealed with paraffin (±0.03 m thick) and wrapped in three layers of aluminum foil. The details of these tests have been published by the authors [17,18].

Table 5 presents the results of this experimental campaign. This table shows the increase in the strain due to shrinkage when the RCA increases its RC content. Similarly, from these results, it is concluded that the creep coefficients report a direct correlation with the increase of the factor r (principally in shrinkage and creep for drying).

2.5. Porosimetry by mercury intrusion

Due to the broad pore size spectrum of the concretes (1 nm–1 cm), it was decided to use the MIP technique, which covers this spectrum to a great extent. It was applied using the ASTM D 4404 standard [34] and the concepts expressed below.

2.5.1. Procedure

The tests were carried out at 7, 28 (samples of concrete submitted to curing chamber conditions to correlate them with physical and mechanical properties of RCs) and 90 days (samples of concrete submitted to climatic chamber conditions to correlate them with shrinkage and creep). The samples for the MIP tests were extracted from the center of the samples (0.10×0.10 m) using a core catcher with a diamond bit. The resulting cylinder (∅=0.02 m × h=0.10 m) was then cut with a fine saw to obtain two central cylinders with dimensions of ∅=0.02 m × h=0.03 m.

The samples for tests at 7 and 28 days were dried by stages: firstly, the samples were dehydrated by submerging them in alcohol for 8 days. The alcohol was changed every 24 h. After this stage, the samples were dried by putting them in an oven at T=70 °C for 24 h. Finally, the samples were put into a drier until the tests.

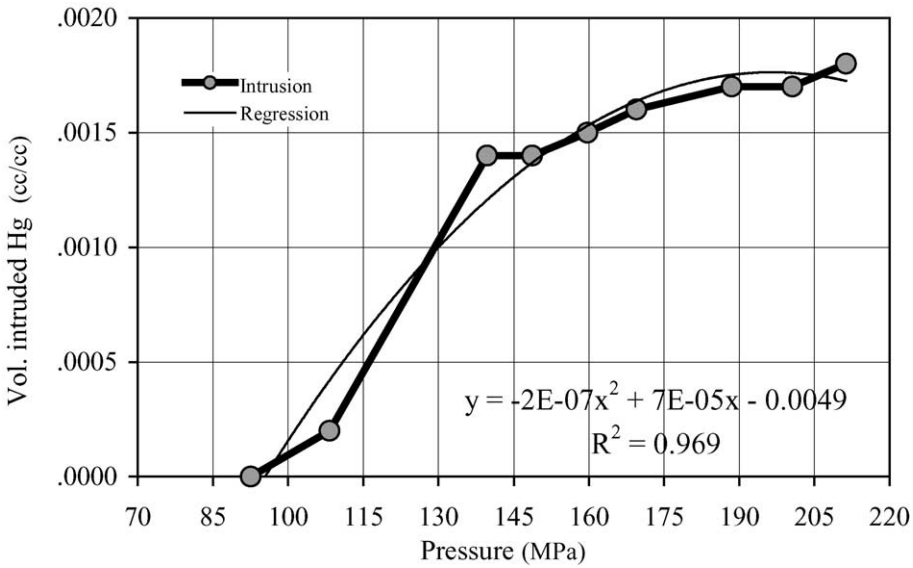

Fig. 1. Distribution in the black test.

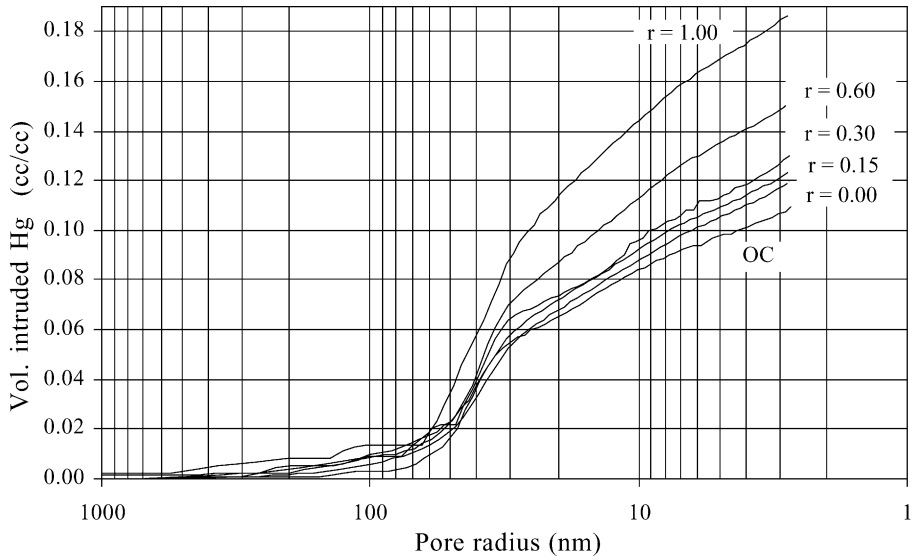

Fig. 2. General distribution (age 7 days).

The samples for the tests at 90 days, after 28 days in the curing chamber, were put in the climatic chamber until the age of 90 days. Upon arriving at this age, the samples were extracted and dried by putting them in an oven at T=120 °C for 24 h, and then in a drier.

The MIP tests were done on a Quantachrome Autoscan 33 porosimeter, which subjected the samples to a maximum pressure of up to 226 MPa. The following parameter was measured: the theoretical pore radius (r_{pt}), within the range 27–59,000 Å (the Washburn equation was used for the calculation). The process included the typical intrusion and extrusion cycles in this type of test. Finally, to improve the profile of the test curve, the sample results were filtered using a moving average with Base 9.

The following constants and hypotheses were applied in this study (for all the samples): mercury (Hg) contact angle with the concrete θ=130°, Hg surface tension σ=0.480 N/m^2, pore shape factor φ=4.00, together with the typical hypotheses of the methodology of this test [35,36].

2.5.2. Corrections applied to the test values [37]

The test values obtained based above were submitted to three corrections to improve their accuracy.

2.5.2.1. Blank test. A test with the dilatometer without a sample was carried out to obtain the volume of Hg that causes the dilatometer to expand, and the compression that

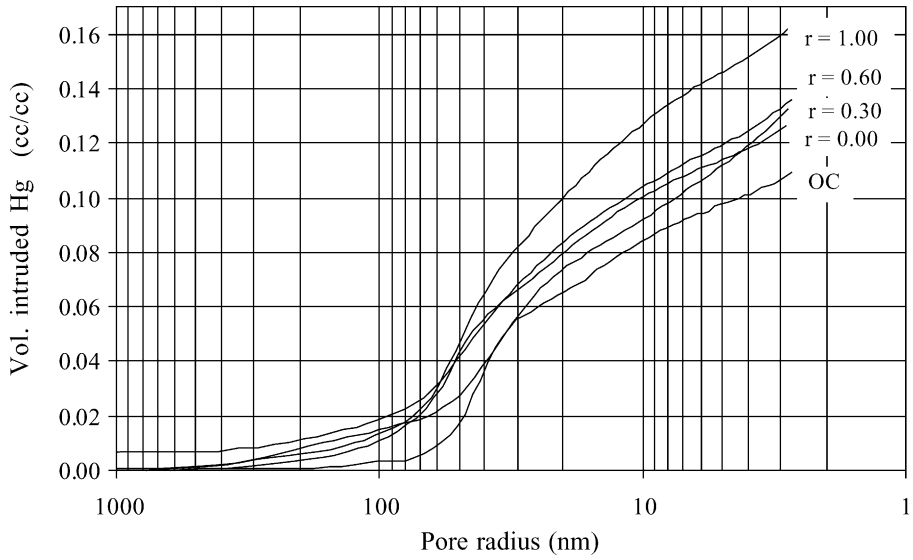

Fig. 3. General distribution (age 28 days).

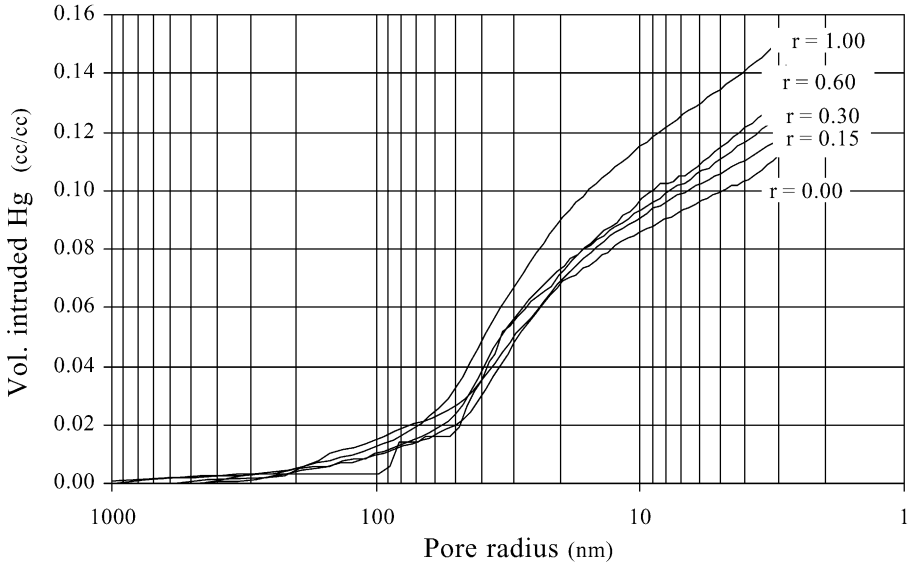

Fig. 4. General distribution (age 90 days).

the Hg undergoes to fill the dilatometer. The following correlation was obtained from this test (see Eq. (1)):

$$V_{\text{blank}} = -2\text{E}^{-07}x^2 + 7\text{E}^{-05}x - 0.0049. \quad (1)$$

The result of the above correlation (V_{blank}) was subtracted from the uncorrected Hg volume of the tests (V_o) when the test pressure (x) was greater than or equal to 92.56 MPa. The blank test and the proposed correlation are shown in Fig. 1.

2.5.2.2. Differential compression of Hg. The sample displaces a volume of Hg equal to the mass of the sample ($\text{BV}_{\text{sample}}$). The blank test, therefore, includes the compression of a volume of mercury (equal to $\text{BV}_{\text{sample}}$) that is not seen in the volume of the experimental test (V''_{cHg}). If the above variables are taken into account, it is possible to determine V''_{cHg} using the following equation (Eq. (2)):

$$V''_{\text{cHg}} = 0.175\text{BV}_{\text{sample}}\log_{10}(1 + (x/1820\ \text{MPa})). \quad (2)$$

2.5.2.3. Compression of the sample. This estimates the compressibility factor of a volume of the sample that was not intruded (V_{cs}). Given the compressibility coefficient of the material (ψ_{sample}, proposed=5.0 E^{-10} m^2/N) and the volume of the sample without intruded Hg ($\text{UV}_{\text{sample}}$), it is feasible to calculate the compression of the sample using the following equation (Eq. (3)):

$$V_{\text{cs}} = x\psi_{\text{sample}}\text{UV}_{\text{sample}}. \quad (3)$$

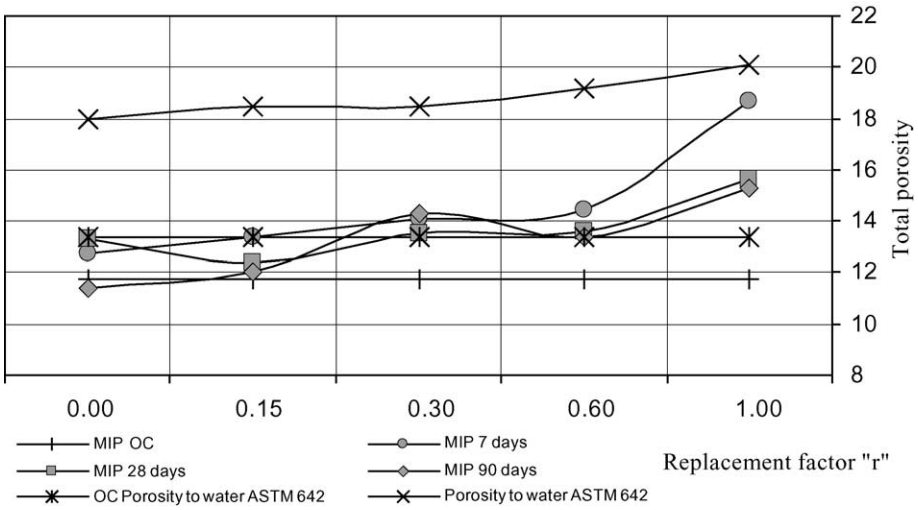

Fig. 5. Total porosity.

Table 6
Critical radius for the different RCs

$r_{critical}$ (nm)									
	dv/d*p* VS pore radius			$\alpha^a > 1'$			$1' < \alpha^a < 5'$		
Method factor	7 days	28 days	90 days	7 days	28 days	90 days	7 days	28 days	90 days
OC	44.70	–	–	63.64[b]	–	–	57.34[b]	–	–
r=0.00	40.31	51.61	38.53	70.39	83.93	62.67	59.76	68.75	51.94
r=0.15	36.50	73.63	40.60	65.17	68.68	57.26	56.21	47.63	46.46
r=0.30	53.88	91.62	40.96	65.50	69.50	67.04	60.15	60.98	56.95
r=0.60	44.45	51.00	48.75	70.01	79.48	97.39	60.24	55.78	93.36
r=1.00	45.87	49.63	43.68	68.78	74.29	78.78	58.40	65.66	64.48
Maximum	53.88	91.62	48.75	70.39	83.93	97.39	60.24	68.75	93.36
Minimum	36.50	49.63	38.53	63.64	68.68	57.26	56.21	47.63	46.46
Average	44.28	63.50	42.50	67.25	75.71	72.63	58.68	59.76	62.64

[a] Angle between two consecutive points (pore radius−volume intruded Hg).
[b] At 262 days of age.

The final equation that was used to calculate the porosity at each point of the tests according to the above corrections was the following (see Eq. (4)):

$$V_{\text{intrusion}} = V_{\text{o}} - V_{\text{blank}} + V''_{\text{cHg}} - V_{\text{cs}}. \quad (4)$$

2.5.3. Results

The following sections present the results and analyses derived from the MIP tests performed on the various concretes in the study.

2.5.3.1. Distribution of the pore radius. Figs. 2–4 show the graphs for the tests carried out at 7, 28 and 90 days for the various concrete samples. To avoid confusion when interpreting the graphs, only the curves of the Hg intrusion stages are presented.

It may be seen from the three graphs that the increase in the *r* factor of the RCs shows a correlation with total porosity, as the latter increases by 5.9% when *r* goes from *r*=0.00 to *r*=1.00 at 7 days, 2.3% for 28 days and 3.8% for 90 days (taken from the three graphs as average values of two tests for each variable).

It is also seen in Fig. 5 that the total porosity decreases appreciably for all the concretes as a function of age. The evolution of total porosity of these concretes amounts to a decrease of 0.5% from 7 to 28 days with the exception of *r*=1.00, which shows a greater reduction (3.0%). Total porosity drops by 0.42% on average upon going from 28 to 90 days, the maximum standing at *r*=1.00 (1.9%).

It should be pointed out that the main difference in the total porosity between the different RCs (*r*=1.00 and the rest of the concretes) is seen in the area with pore radius less than 30 nm (the zone of maximum percentage of pore volume in the concretes and originating in the cement mortar). It is also in this zone that the decrease in porosity with age is seen. The above pore range is commonly associated with the power to damage the dimensional stability and influence the mechanical properties of the concretes [38].

2.5.3.2. Critical pore radius. Characteristic radius or critical pore (r_{critical}) is the term given to the corresponding radius that causes the beginning of the maximum slope in the curve of the radius versus volume of the intruded Hg graph. This pore radius is usually an indicator of the microstructure of the material and it is used to detect a variety of materials. For the determination of this parameter, two different methods were used as follows:

(i) Calculate the angle between two consecutive points (α) of all the values that take in all of the curves in the study. The criteria for establish distinction were the following: (a) pore radius that causes the first angle that is greater than 1° of elevation in the slope of the curve under study; and (b) the average pore radius range that generates an angle of elevation between 1° and 5° of the beginning of elevation of the curve under study.

(ii) Point maximum peak of the named curve of frequencies density dv/d*p* (cm^3/MPa cm^3) VS pore radio (nm).

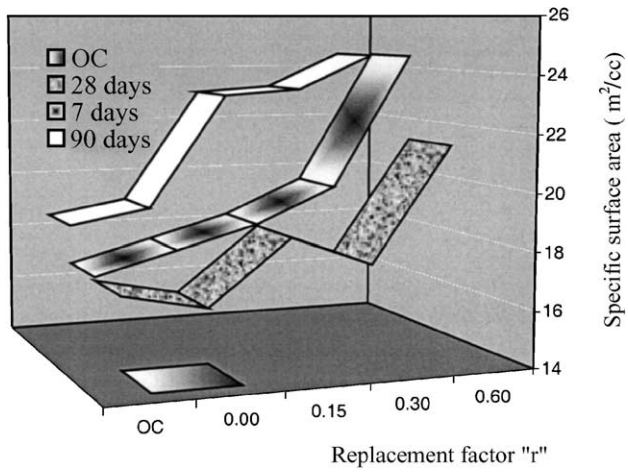

Fig. 6. Specific surface area for RC.

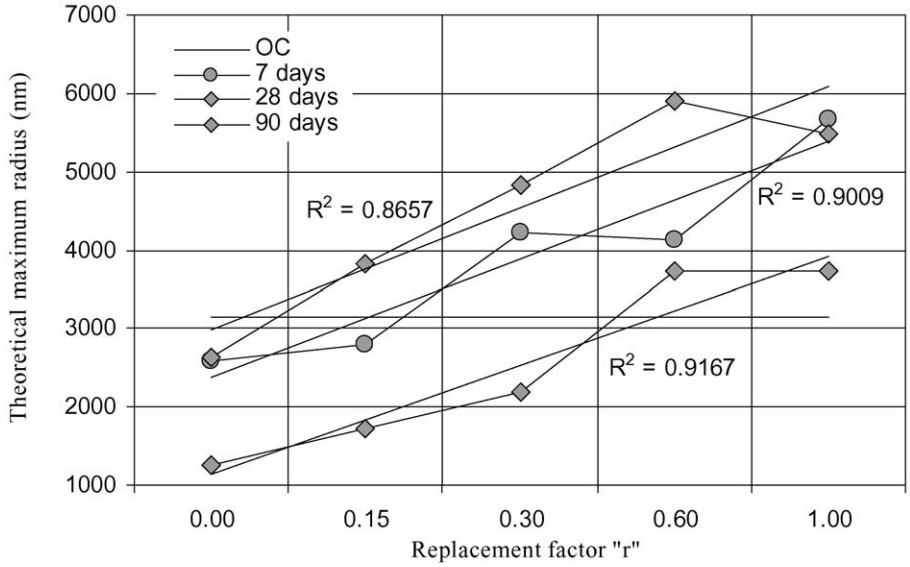

Fig. 7. Maximum pore radius.

Table 6 shows the critical pore radius calculated as explained above. As is seen, the values in the tests are approximately 36–97 nm (with a population average of 60.46 nm), which locates these pores in the range of large capillary or macropores (50–10,000 nm); at this capillary range, negative effects that can affect the strength and the impermeability of a concrete can be attributed to the pore size. However, the difference between the different $r_{critical}$ of the concretes studied is negligible as the variation between them is small. With respect to the two methods for its determination, the most exact is critical pore radius; however, Case (i,b) is of greater importance due to the ease with which it determines $r_{critical}$ and the fact that it presents a mean variation with respect to critical pore radius of only 15%.

2.5.3.3. Specific surface area. The MIP technique enables the determination of the surface area of the material from direct sampling of the pressure versus volume of intruded Hg (Fig. 6). The method does not require previous knowledge of the geometry of the pore, which means that its results are reliable. However, the maximum level of available pressure of the porosimeter used cannot guarantee intrusion of all the pore sizes that cover the specific surface of the samples and it is not possible to evaluate whether high levels of pressure cause crushing of sealed pores.

The observed general behavior is an increase (important for the case of $r=1.00$) in agreement with the increase of the r factor. For this property, the results do

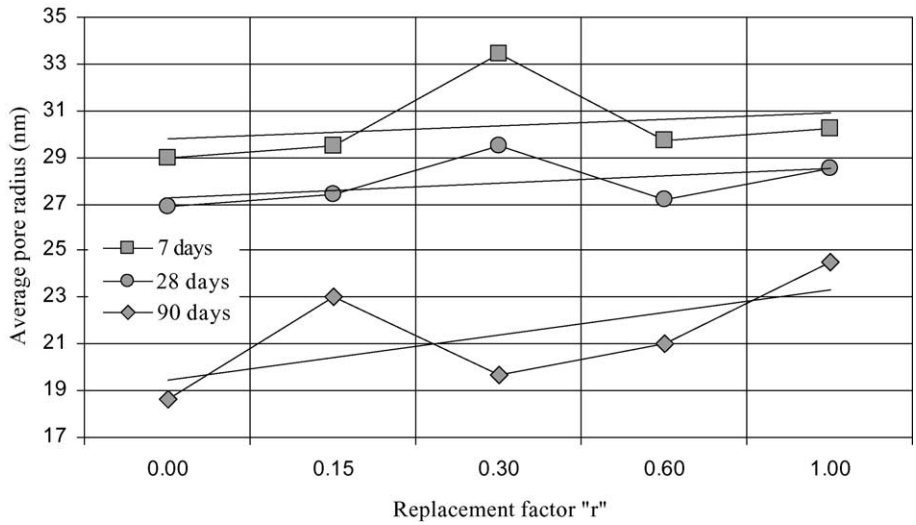

Fig. 8. Average pore radius.

Table 7
Correlation between total porosity and other properties of the RCs

Property	Equation[a]	R^2
Absorption (%)	$y=0.3501x+4.0460$	.7641
Porosity to water (%)	$y=0.5714x+11.036$	.7000
D_s (t/m^3)	$y=-0.0165x+2.3514$	.7267
D_{sss} (t/m^3)	$y=-0.0191x+2.5836$	.7745
Permeability (cm)		
Average	$y=0.1564x-1.3955$	.7652
Maximum	$y=1.0006x-1.3819$	.6076
f_t (MPa)	$y=0.0185x^2-0.6527x+8.9077$	.5727
f_c' (MPa)	$y=0.3744x^2-12.906x+141.05$	.7350
E (GPa)	$y=0.1984x^2-6.395x+77.316$	.6510
$\varepsilon_{sh\ drying}$ (mm/m)	$y=2E^{-08}z^2-9E^{-05}z+0.4607$	.8367
φ (90 $_{days}$, t_0)	$y=-3E^{-07}z^2+0.0019z+1.0833$	.9347

[a] x=total porosity in (%) MIP; z=pore threshold (nm).

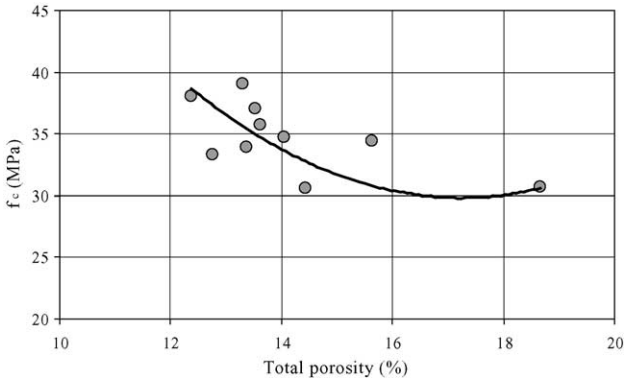

Fig. 10. Total porosity versus compressive strength.

not present a logical correlation with the age of the specimens, which maybe related to the fact that the samples were submitted to two types of environmental conditions and two drying processes.

2.5.3.4. Pore threshold. This name is given to the maximum pore radius found (either in the intrusion or extrusion stage) in the MIP test [39]. Fig. 7 shows the maximum radius for the concretes studied.

Correlations for the three curves are fairly high. However, the interpretation and usefulness of this parameter can only serve as a guideline, as its determination involves a high degree of uncertainty.

2.5.3.5. Average pore radius. Pore radius ($r_{average}$) is the name given to the radius that corresponds to 50% of the total volume of Hg intruded in the test. In Fig. 8, the $r_{average}$ calculated through the Lagrange interpolation of the two nearest points to 50% of the total volume for each sample is presented.

The presented behavior of $r_{average}$ is correlative with the age of the samples, as well as with the r factor (in this last case in smaller proportion).

2.5.4. Correlation between porosity and properties of the concretes

The correlation process was carried out on the properties obtained from the MIP tests, the physical and mechanical properties of the RCs (7 and 28 days), and shrinkage and creep (90 days). The processed data were examined with different lines of tendency, in which different correlation coefficients (R^2) were used as indicators of greater reciprocity between the variables.

Table 7 shows the correlation equations for the total porosity data and the physical properties of the RCs. The correlations only include MIP tests for 28 days, as the physical tests were done at this time. The table also shows the correlation for total porosity and mechanical properties of the RCs (the correlations are an average of tests at 7 and 28 days). Finally, the correlation equations between shrinkage and the creep coefficient with the MIP tests for 90 days are also presented.

Figs. 9–11 show the graphs that gave rise to the correlations of the mechanical properties and the total porosity obtained in the MIP tests.

Total porosity, obtained from the MIP tests, is the property that showed the best correlation for the behavior

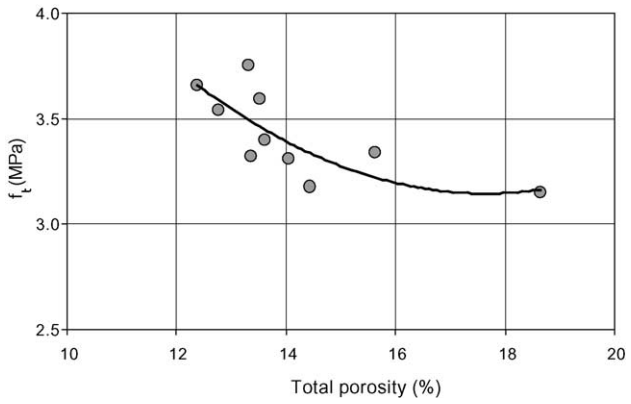

Fig. 9. Total porosity versus tensile strength.

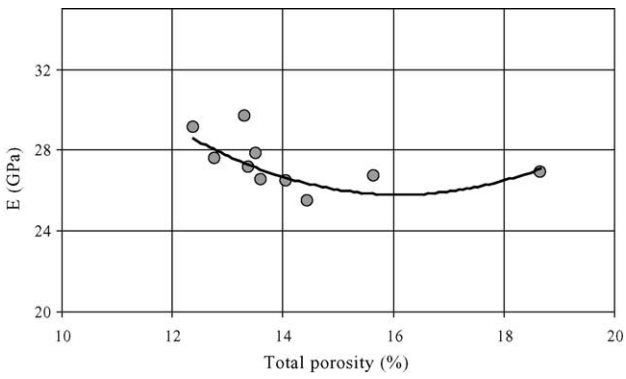

Fig. 11. Total porosity versus Young's modulus.

of the studied concretes, followed by the specific surface area, $r_{critical}$, the pore threshold radius and, lastly, $r_{average}$.

As regards the types of lines of tendency used, the physical properties follow the pattern of linear correlation better than the mechanical properties, while the mechanical properties fit quadratic-type equations better. This latter fact may indicate that these equations could be improved if other factors (in addition to total porosity) of similar importance are taken into account, such as the increase in the interface zones (which favors the formation and propagation of microcracks) and a major variation in the distribution of the pore radius (especially in the zone of pore radius <30 nm). In both cases, the cause of these new factors to be considered in RCs is the old mortar that adheres to the NA of which the RCA is composed.

3. Conclusions

Based on the research and results presented in this paper, the following conclusions are reached.

• The replacement factor r of the RCs shows a correlation with total volume and pore size, its influence being more important at lower ages and diminishing as the concrete ages. This influence is attributed to the crystallization of new products that reduce both the number and size of the pores.

• The most significant differences of the studied samples are seen in two parameters: (1) the greater pore radius threshold as the replacement of NA by RCA is increased; and (2) the detection of zones of major quantitative changes seen in the increase of the pore volume from pores with radius <30 nm.

• The effect of the r factor does not seem to influence the $r_{critical}$ values, and therefore, this parameter may be used only in cases in which determination of the variation of structural components of the concrete that was used for the RCA is desired, and whose probable cause of variation would be the modification of the physical constants of the concretes (W/C, type of cement, etc.).

• The results for specific surface area, together with total porosity, are those which better describe and correlate the results of the properties of the studied concrete. However, it will be necessary to supplement this information with tests of gas absorption, which would enable quantification of the surface area in the micropore zone and thus be able to better correlate these tests with other properties such as shrinkage and creep; both are linked to the distribution and quantity of micropores.

• Finally, correlation between the properties of the RC and total porosity is difficult to determine. However, it would be feasible to improve it if the distribution of the pore radius was included. This distribution could be ascertained by classifying boundaries between different ranges of pore size, taking as a classification criterion the effect of size on the behavior of the property of the RC under study. It would also be advisable to include parameters that evaluate the formation and propagation of microcracks in the interface zones, as these zones (mechanically weaker than the mortar) increase in the RCs due to the replacement of NA by RCA.

Acknowledgments

The author would like to express their gratitude to the company Cervezas Finas de Cd. Serdán, Puebla, Mexico, for the partial financing of this research; to the Technical University of Catalonia, Barcelona, Spain, for the use of their facilities; and to Drs. L. Agulló and E. Vázquez.

References

[1] J. Bjϕrn-Jakobse, M. Elle, E.K. Lauritzen, On-site use of regenerated demolition debris, in: Y. Kasai (Ed.), Demolition and Reuse of Concrete and Masonry, Reuse of Demolition Waste, vol. 2, E&FN SPON, London, 1988, pp. 537–546.

[2] W. Grübl, Environmentally Friendly Construction Technology—Interaction Between Construction and Environment (1999) (http:www.b-i-m-de/public/Tudmassiv/dacon98gruebl.htm).

[3] T.C. Hansen, Recycled of demolished concrete and masonry, Report of Technical Committee 37-DRC Demolition and Reuse of Concrete, Part 1, E&FN SPON, London, 1992, pp. 1–160.

[4] T.C. Hansen, E. Bϕegh, Elasticity and drying shrinkage of recycle-aggregate, ACI J. (5) (1995) 648–652.

[5] T.C. Hansen, M. Marga, Strength of recycle made from coarse and fine recycled concrete aggregates, in: Y. Kasai (Ed.), Demolition and Reuse of Concrete and Masonry, Reuse of Demolition Waste, vol. 2, Chapman & Hall, London, 1988, pp. 605–612.

[6] M. Kakizaki, M. Harada, T. Soshiroda, S. Kubota, T. Ikeda, Y. Kasai, Strength and elastic modulus of recycled aggregate concrete, in: Y. Kasai (Ed.), Demolition and Reuse of Concrete and Masonry, Reuse of Demolition Waste, vol. 2, Chapman & Hall, London, 1988, pp. 565–574.

[7] E.K. Lauritzen, M. Jannerup, Guidelines and experience from the demolition of houses in connection with the resound Link between Denmark and Sweden, Demolition and Reuse of Concrete and Masonry, in: E.K. Lauritzen (Ed.), Guidelines for Demolition and Reuse of Concrete and Masonry, E&FN SPON, Denmark, 1993, pp. 35–46.

[8] P.J. Wainwright, A. Trevorrow, Y. Yu, Y. Wang, Modifying the performance of concrete made with coarse and fine recycled concrete aggregates, in: E.K. Lauritzen (Ed.), Demolition and Reuse of Concrete and Masonry, Guidelines for Demolition and Reuse of Concrete and Masonry, E&FN SPON, Denmark, 1993, pp. 319–330.

[9] A. Müeller, A. Winkler, Characteristics of processed concrete rubble, in: K.R. Dhir, N.A. Henderson, M.C. Limbachiya (Eds.), Uses of Recycled Concrete Aggregate. Sustainable Construction, Tomas Telford, London, 1998, pp. 1109–1119.

[10] P.J. Wainwright, J.G. Cabrera, Use of demolition concrete to produce durable structural concrete, in: J.J.J.M. Goumans, H.A. Van Der Sloot, T.G. Aalbers (Eds.), Environmental Aspects of Construction with Waste Materials, Elsevier, The Netherlands, 1994, pp. 553–562.

[11] B. Zhang, Relationship between pore structure and mechanical properties of ordinary concrete under bending fatigue, Cem. Concr. Res. 28 (5) (1998) 699–711.

[12] H. Uchikawa, S. Hanehara, Recycling of concrete waste, in: R.K. Dhir, T.D. Dyer (Eds.), Concrete for Environment Enhancement and Protection, E&FN SPON, London, 1996, pp. 163–172.

[13] C.F. Hendriks, Certification system for aggregates produced from

building waste and demolished buildings, in: J.J.J.M. Goumans, H.A. Van Der Sloot, T.G. Aalbers (Eds.), Environmental Aspects of Construction with Waste Materials, Elsevier, Amsterdam, The Netherlands, 1994, pp. 821–843.
[14] J. Kasai, Y. Kasai, Guidelines and the present state of the reuse of demolished concrete in Japan, in: E.K. Lauritzen (Ed.), Demolition and Reuse of Concrete and Masonry, Guidelines for Demolition and Reuse of Concrete and Masonry, 1993, pp. 93–104 (Odense, Denmark).
[15] RILEM Recommendation, 121-DRG Guidance for demolition and reuse of concrete and masonry. Specifications for concrete with recycle aggregates, J. Mater. Struct. 27 (1994) 557–59.
[16] J. Vyncke, E. Rousseau, Recycling of construction and waste in Belgium: actual situation and future evolution, in: E.K. Lauritzen (Ed.), Demolition and reuse of concrete and masonry, Guidelines for Demolition and Reuse of Concrete and Masonry, E&FN SPON, Denmark, 1993, pp. 57–69.
[17] J.M. Gómez, E. Vázquez, L. Agulló, Strength and deformation properties of recycled aggregate concrete, Fifth CANMET/ACI International Conference on Recent Advances in Concrete Technology, Singapore, 2001, pp. 103–120 (Supplementary papers; M. Venturino (Compiler)).
[18] J.M. Gómez, L. Agulló, E. Vázquez, Cualidades físicas y mecánicas de los agregados reciclados de concreto. Construcción y Tecnología. Magazine of the Mexican Institute of the Cement and the Concrete, AC (IMCYC), Mexico, DF, Mexico, Vol. XIII (157) (2001) pp. 10–22 (ISSN 0187-7895) (In Spanish) http://www.imcyc.com/cyt/junio/cualidades.htm.
[19] J.M. Gómez, E. Vázquez, L. Agulló, Hormigón con áridos reciclados. Una guía de diseño para el material. International Center of Numerical Methods in Engineering (CIMNE). Monograph M60 (2001) 1–137 (ISBN 84-89925-80-1), Barcelona, Spain (in Spanish).
[20] J.M. Gómez, L. Aguyó, E. Vázquez, Repercussions on concrete permeability due to recycled concrete aggregate, in: V.M. Malhotra (Ed.), Third CANMET/ACI International Symposium on Sustainable Development of Cement and Concrete, San Francisco, USA, 2001, pp. 181–195 (ISBN 0-87031-041-0; SP 202–13).
[21] UNE 7083, Determinación del peso específico y de la absorción en gravas y arenas, AENOR (Asociación Española de Normalización y Certificación), 1954 (in Spanish).
[22] UNE 7140, Determinación de los pesos específicos y absorción de agua en áridos finos, AENOR (Asociación Española de Normalización y Certificación), 1958 (in Spanish).
[23] UNE 7238, Determinación de coeficiente de forma del árido grueso empleado en la fabricación de hormigones, AENOR (Asociación Española de Normalización y Certificación), 1971 (in Spanish).
[24] UNE 83.116, Áridos para hormigón, Determinación del coeficiente Los Ángeles, AENOR (Asociación Española de Normalización y Certificación), 1990 (in Spanish).
[25] UNE 83.131, Áridos para hormigones, Determinación del equivalente de arena, AENOR (Asociación Española de Normalización y Certificación), 1990 (in Spanish).
[26] UNE 83.133, Áridos para hormigones, Determinación de las densidades, coeficientes de absorción y contenido de agua en el árido fino, AENOR (Asociación Española de Normalización y Certificación), 1990 (in Spanish).
[27] UNE 83.134, Áridos para hormigones, Determinación de la densidad, porosidad, coeficiente de absorción y contenido en agua del árido grueso, AENOR (Asociación Española de Normalización y Certificación), 1990 (in Spanish).
[28] UNE 83.304, Ensayos de hormigón, Rotura por compresión, AENOR (Asociación Española de Normalización y Certificación), 1984 (in Spanish).
[29] UNE 83.306, Ensayos de hormigón, Rotura por tracción indirecta (Ensayo Brasileño), AENOR (Asociación Española de Normalización y Certificación), 1985 (in Spanish).
[30] UNE 83.310, Ensayos de hormigón, Determinación de la permeabilidad, AENOR (Asociación Española de Normalización y Certificación), 1990 (in Spanish).
[31] UNE 83.312, Ensayos de hormigón. Hormigón endurecido, Determinación de la densidad, AENOR (Asociación Española de Normalización y Certificación), 1990 (in Spanish).
[32] UNE 83.316, Ensayos de hormigón, Determinación del módulo de elasticidad en compresión, AENOR (Asociación Española de Normalización y Certificación), 1996 (in Spanish).
[33] UNE-EN 933:3, Ensayos para determinar las propiedades mecánicas y físicas de los áridos: Parte 3. Determinación de la forma de las partículas. Índice de lajas, AENOR (Asociación Española de Normalización y Certificación), 1997 (in Spanish).
[34] ASTM D 4404, Determination of pore volume and pore volume distribution of soil and rock by mercury intrusion porosimetry. P.A., United States of America, 1998.
[35] F.G. Rodríguez, Porosimetría por intrusión de mercurio: Fundamentos de la técnica y aplicación a la caracterización microestructural de hormigones, Ing. Civ. (1997) 21–37 (in Spanish).
[36] S. Diamond, Methodologies of PSD measurements in HCP: Postulates, peculiarities, and problems, in: L.R. Roberts, J.P. Skalny (Eds.), Pore Structure and Permeability of Cementitious Materials, Symposium Proceedings vol. 137, Materials Research Society, Pittsburgh, United States of America, 1989, pp. 83–89.
[37] A. Raymond, A. Cook, K.C. Hover, Mercury porosimetry of cement-based materials and associated correction factors, ACI Mat. J. (1993) 152–161.
[38] D.A. St. John, A.W. Poole, I. Sims, Concrete petrography, A Handbook of Investigative Techniques, Arnold, London, 1998, pp. 1–474.
[39] R.F. Felddman, The porosity and pore structure of hydrated Portland cement paste, in: L.R. Roberts, J.P. Skalny (Eds.), Pore Structure and Permeability of Cementitious Materials, Symposium Proceedings, vol. 137, Materials Research Society, Pittsburgh, United States of America, 1989, pp. 59–73.